

Exploring the Formation Mechanisms of Double Neutron Star Systems: An Analytical Perspective

Ali Taani ¹, Mohammed Abu-Saleem ², Mohammad Mardini ^{3,4}, Hussam Aljboor⁵, and Mohammad Tayem¹

¹ Physics Department, Faculty of Science, Al-Balqa Applied University, Al-Salt 19117, Jordan

² Mathematics Department, Faculty of Science, Al-Balqa Applied University, Salt 19117, Jordan

³ Department of Physics, Zarqa University, Zarqa 13110, Jordan

⁴ Department of Physics and Kavli Institute for Astrophysics and Space Research, Massachusetts Institute of Technology (MIT), Cambridge, MA 02139, USA

⁵ Department of Basic Scientific Sciences, Prince Hussein Bin Abdullah II Academy for Civil Protection, Al Balqa applied university, Amman, Jordan

The dates of receipt and acceptance should be inserted later

Key words stars: binaries — stars: pulsars — stars: neutron — stars: fundamental parameters, Core-Collapse and Electron-Capture Supernovae

Double Neutron Stars (DNSs) are unique probes to study various aspects of modern astrophysics. Recent discoveries have confirmed direct connections between DNSs and supernova explosions. This provides valuable information about the evolutionary history of these systems, especially regarding whether the second-born Neutron Star (NS) originated from either a Core-Collapse (*CC*) or Electron-Capture Supernovae (*ECSNe*) event. The provided scale diagram illustrates the distribution of different types of DNSs on the basis of their orbital parameters and other factors, including mass loss. As a result, the physical processes in DNSs vary depending on the formation mechanisms of the second-born NS and characteristics of the systems. *ECSNe* processes are typically associated with merging systems ($e \times P_{orb} < 0.05$), while *CC* processes are more commonly linked to non-merging systems ($e \times P_{orb} > 0.05$). Our results suggest a critical mass threshold of $1.30M_{\odot} \pm 0.22M_{\odot}$ (critical value) for the *ECSNe* process to form an NS, while *CC* processes might occur at higher masses. Examining the orbital parameters of DNSs in a known gravitational potential can enhance our understanding of the theoretical predictions for DNS progenitor characteristics. It turns out that the *ECSNe* process predominantly produces DNS systems with short orbital ($P_{orb} \leq 0.25d$), nearly circular orbits ($e \simeq 0.2$), accompanied by minimal kick velocities imparted on the proto-NS and significant mass loss. In contrast, their orbital dynamics in a known gravitational potential plays a crucial role in enhancing our understanding of the SNe geometry and the formation and evolution processes among different NS samples.

Copyright line will be provided by the publisher

1 Introduction

Chronologically, double neutron star (DNS) systems represent the endpoint of the evolution of two massive main-sequence stars. However, DNSs are formed by distinct methods in both electron-capture supernovae (*ECSNe*) and core-collapse (*CC*) events [Stairs et al., 2006, Tauris and van den Heuvel, 2023, Tauris et al., 2017, Wang et al., 2006, Yang et al., 2017b]. In the case of *ECSNe*, a system composed of two massive main sequence stars may form a *ONeMg* core after burning of carbon [Podsiadlowski et al., 2005]. The *ONeMg* core has an upper mass of $1.37 M_{\odot}$ and a lower He core mass ($\sim 2 M_{\odot}$). *CC* SNe in massive stars (ranging from $12\text{-}25M_{\odot}$) with iron cores cause implosions [Taani, 2023, Wong et al., 2010], generating significant energy that compresses the core, often leading to the formation of DNSs. Further detailed discussions can be found in Sec. 3, and their physical parameters in Table 1. Researchers pay particular attention to DNSs; because a notable fraction of them are detected as radio pulsars [Dewi et al., 2006, Galadage et al., 2021, Zhu and Ashton, 2020]. In addition,

DNSs play a crucial role in the detection of gravitational waves, their collision rates and NS interiors [Abbott et al., 2016, Clark et al., 2016, Kim et al., 2015, Tauris et al., 2017, van den Heuvel, 2010], also are thought to be the primary drivers behind the majority of short-Gamma bursts [Ding et al., 2024]. PSR J0737-3039AB, a binary system with a recycled NS, offers a valuable source for conducting extraordinary investigations into fundamental physics, indicating a possible (recycled) formation history from a close helium star in an NS binary [e.g., Burgay et al., 2003, Lyne et al., 2004]. Furthermore, DNSs offer the opportunity to place observational constraints on some fundamental scientific aspects, such as empirical rate estimates, including the phase of mass transfer through Roche-lobe overflow at a high rate. Kim et al. [2015] argue that the non-recycled NS binary J1906 + 0746 significantly constrains the uncertainties associated with the empirical rate estimates by increasing the Galactic DNS merger rate by a factor of two. In general, DNSs have been demonstrated to be marvelous systems for the study of Einstein's theory of general rela-

Copyright line will be provided by the publisher

tivity, the prediction of gravitational-waves and the strong-field regime through long-term timing observations [Abbott et al., 2017b, Borhanian, 2024, Kalogera et al., 2021, Kramer et al., 2021, McClelland et al., 2021].

To justify the classification of SNe into CC and EC-SNe types, we present several key criteria based on empirical evidence and theoretical frameworks. First, we specify the progenitor mass ranges: *CC* typically arise from stars with ZAMS masses $12 - 25M_{\odot}$ [Dewi et al., 2006, Yang et al., 2017a], while the *EC*SNe progenitor lie in the range of approximately $8 - 12M_{\odot}$ van den Heuvel [2010]. Second, we outline the distinct evolutionary pathways for each type: *CC* result from the formation of an iron core, whereas *EC*SNe originated from electron-capture processes occurring in the degenerate ONeMg cores of intermediate-mass stars Tauris et al. [2015]. Additionally, we incorporate observational evidence supporting the existence of these supernova classes, including statistics on the mass distributions and physical properties of the NSs formed from each SNe type. We also highlight the key characteristics of these NSs, noting differences in mass, spin period, and magnetic field strength. Finally, we present a statistical analysis demonstrating the significance of these distinctions, reinforcing the classification is grounded in empirical data and theoretical understanding rather than arbitrary assumptions.

The kick velocity of an NS is caused by the ejection of asymmetric material during the explosion of SNe [Podsiadlowski et al., 2004, Taani et al., 2022a,b]. Typically, these velocities range between 100-500 km/s, although it can reach up to 1000 km/s in some cases for *CC* [Podsiadlowski et al., 2004]. *EC*SNe process mainly lead to DNS with tight, circular orbits, low kick velocity due to the near-spherical symmetry of the explosion and lower mass ejection [Wong et al., 2010]. In addition, the *EC*SNe process could be particularly important in producing compact binaries that include a NS [Kruckow et al., 2018, Zha et al., 2022]. DNSs exhibit a wide range of orbital eccentricities (see Table 2). The magnitude and direction of asymmetric kicks present uncertainties in stellar population synthesis. More models are required to characterize all binary parameters. The loss of angular momentum due to orbital decay leads to a process known as in spiral [Dai et al., 2017], increasing the merger event rates of DNS, making them one of the best-characterized sources of gravitational wave for multi-messenger observations [e.g., Abu-Saleem and Taani, 2021a, Borhanian, 2024, Shappee et al., 2017, Taani and Vallejo, 2017]. [Colom Bernadich et al., 2023] More recently, [Abbott et al., 2017b] confirmed the connection between DNS and the short γ ray burst by observing GW170817. The merging of DNS can be measured by gravitational waves, which can provide cosmological information, implications, distances, and even extend to our understanding to the edge of the universe [e.g., Abbott et al., 2017a].

To date, over 100 gravitational wave events have been confidently reported in the GWTC-3 and 4-OGC catalogs, following the first three observing runs (O1–O3) conducted

by the LIGO–Virgo–KAGRA collaboration Acernese and et al. [2023], Nitz et al. [2023]. The majority these detection involve binary black hole mergers, while a smaller fraction consists of binary neutron star and neutron star–black hole systems (Abbott and et al. [2023], Koloniari et al. [2025]). The LIGO and Virgo detectors have observed the first gravitational waves from two DNS systems in the events GW170817 [Abbott et al., 2017b] and GW190425 [Abbott et al., 2020]. However, many more DNS systems are expected to be observed through gravitational waves in the near future. The literature on DNS classifications and their formation mechanisms is extensive and interesting. In Burgay et al. [2021], Chattopadhyay et al. [2020], Lasky [2015], Miller and Yunes [2019], Tauris and van den Heuvel [2023], Wex [2017], the researchers included the modeling of DNSs as probes for general relativity and gravitational wave relativity. Interested readers are encouraged to refer to the provided references for a detailed review Abu-Saleem and Taani [2021b], Aljboor and Taani [2023], Andrews et al. [2015], Galaudage et al. [2021], Mardini et al. [2020], Taani and Khasawneh [2017], Taani et al. [2012a,b], van den Heuvel [2007], Wang et al. [2006], Wong et al. [2010], Zhu and Ashton [2020] and the references therein for a detailed review.

The structure of the paper is organized as follows. We describe the observational sample, in Sect. 2. In Sect. 3, the two evolutionary models are introduced. Sect. 4 we will analyze the dynamical properties of a set of DNSs. We will describe the mass of non-recycled NSs and the relationship of eccentricity and orbital period. The final goal is to discover a better classification method with respect to the companion mass and orbital parameters. Finally, we will end with some discussions and conclusions in Sect. 5.

2 The observational sample

The DNS systems observed in our galaxy include 24 that reside in the galactic disk and the remaining eight in globular clusters (B2127+11C in NGC 7078, J1807-2500B in NGC 6544, J2140-2311B in NGC 7099, J1835-3259A in NGC 6652, J1748-2021B in NGC 6440, J1748-2446ao in Terzan 5, J0514-4002E in NGC 1851 and J0514-4002A in NGC 1851). We have collected relevant published data on DNS residing in the Galactic disk, as shown in Table 2. Fig. 1 shows the spatial distribution of the current sample of all known DNS systems throughout the Galaxy. The scale-height of the systems is somewhat complex and uniformly distributed. The map of spatial distribution is depicted in Fig. 1, which will aid the preliminary understanding of the distribution of the Electron-Capture Supernovae (*EC*SNe) or Core-Collapse (*CC*), as we can see in Fig. 2.

The detailed analysis of these pulse profiles and their geometric structures was performed by Podsiadlowski et al. [2004, 2005], Tauris et al. [2017], Yang et al. [2017a]. They found that the supernova formed by the second pulsar was relatively symmetric with low mass-loss. They also sug-

gested that, candidates are probably forming in an *ECSNe*, or possibly the collapse of a low-mass iron core.

In the case of PSR J1906+0746, the non-recycled companion suggests that it could be another (as in the DNS system) or a massive white dwarf (as in the NS-WD system). However, the low mass ($1.29M_{\odot}$) of the companion, together with its young age (113 Kyr) and magnetic field (10^{12} G), makes it difficult to detect radio emission from the companion Yang et al. [2017b]. It is possible that there is an unseen recycled pulsar in the system, which could explain the absence of observed radio emission. More research and analysis are needed to fully understand this issue.

A comparative analysis of the physical parameters of PSR J0737-3039B (e.g. orbit eccentricity, spin down age, and the relatively high magnetic field) suggests that this pulsar can be considered as one of the components of the young DNS binary [Kasian, 2008, Kramer et al., 2021, Yang et al., 2017b], forming in an *ECSNe* [van Leeuwen et al., 2015, Yang et al., 2017b]. Another case involves the low companion mass ($1.23M_{\odot}$) PSR J1756-2251, which was discovered by Faulkner et al. [2005] and is believed to have an evolution scenario for the second NS, similar to that of PSR J0737-3039B, indicating an involvement in an *ECSNe* [Ferdman et al., 2014]. The relatively small eccentricity of the PSR J0453+1559 system, compared to other relatively small kick velocities at birth [Cheng et al., 2013, Martinez et al., 2015, Taani, 2016], and the large mass asymmetry are consistent with the formation via *ECSNe*. Lazarus et al. [2016] discovered the massive PSR J1913+1102 system with a maximum total mass ($2.875M_{\odot}$) and an approximately circular trajectory ($e = 0.09$). Furthermore, Ng et al. [2015] discovered PSR J1755-2550, a young radio pulsar with a period of ($P = 315$ ms) in a tight binary system with an orbital period of ($P_{orb} = 9.7$ d). However, the nature of this system remains unclear. More recently, further studies of this system have suggested that it is a DNS system, which may be similar to low eccentricity systems Tauris et al. [2017].

Table 1 A simple statistic of key property ranges of DNS systems.

Parameter ranges of <i>ECSNe</i> NSs:	
Progenitor mass	$8 - 12 M_{\odot}$
Mass, M_p	$1.25 - 1.68 M_{\odot}$
Mean Mass, M_p	$1.39 M_{\odot} \pm 0.22M_{\odot}$
Spin period, P_s	$144 - 2773$ ms
eccentricity, e	$0.085 - 0.181$
Surface dipole B-field, B	$\sim 1 \times 10^{9-10}$ G
Parameter ranges of CC NSs:	
Progenitor mass	$12 - 25 M_{\odot}$
Mass, M_p	$1.31 - 1.79 M_{\odot}$
Mean Mass, M_p	$1.52M_{\odot} \pm 0.15M_{\odot}$
Spin period, P	$22.70 - 185.52$ ms
eccentricity, e	$0.139 - 0.82$
Surface dipole B-field, B	$\sim 1 \times 10^{11-13}$ G

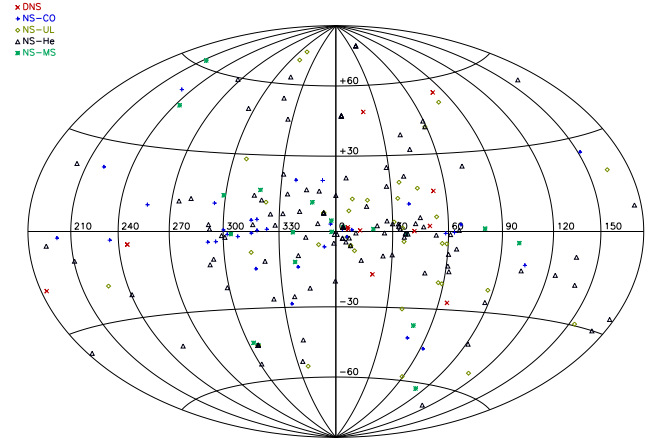


Fig. 1 The spatial distribution of five types of binary systems, NS-NS, NS-CO (NS and CO White Dwarf), NS-UL (NS and uncertain type star), NS-He (NS and He White Dwarf) and NS-MS (NS and main sequence star), is depicted. The red crosses represent DNS. The pulsar data are taken from ATNF pulsar catalogue [Manchester et al., 2005].

Table 2 lists detailed fundamental parameters for known DNSs— including pulsar ID, mass of recycled pulsar (M_p), mass of non-recycled pulsar (M_c), magnetic field (B), orbital period (P_{orb}), spin period (P_s), eccentricity (e), and the corresponding references. As we mentioned in the table, we divided the DNSs into two groups based on eccentricity and orbital period. A specific criterion $e \times P_{orb} = 0.05$ is used to distinguish between these classes. In contrast to systems with $e \times P_{orb} < 0.05$ falling in the region of indicative of merging systems (see [Ferdman et al., 2020]), they exhibit low eccentricity and short orbital periods, suggesting that they were formed by the *ECSNe* process. Systems with $e \times P_{orb} > 0.05$ belong to a distinct region with a large eccentricity and long orbital periods, reflecting more eccentric orbits due to the significant velocities imparted during the explosion (see [Podsiadlowski et al., 2004]). It shows that it forms by CC processes. This classification is determined by the supernova kick velocity and the nature of the binary system partners [Stairs et al., 2006, Tauris and van den Heuvel, 2023, Tauris et al., 2017, Yang et al., 2017b]. It should be noted that among the eight pairs of DNS (B1534+12, B1913+16, J1518+4904, J1829+2456, J1930–1852, J1811–1736, J1753–2240 and J1411–2551), the NS in these systems is believed to have formed through core collapse [Shao and Li, 2018, Weisberg and Huang, 2016]. This conclusion is based on their relatively long orbital periods with high eccentricities and a companions mass of approximately $1.30M_{\odot} \pm 0.22M_{\odot}$.

3 DNS Evolutionary Scenario

Numerous authors have thoroughly studied the formation of DNS systems [Ding et al., 2024, Stairs et al., 2006, Su

Table 2 Parameters of DNS are provided from observations of pulsars in the Milky Way.

System	$M_p(M_\odot)$	$M_c(M_\odot)$	$B(\times 10^9 G)$	$P_{orb}(d)$	$P_s(ms)$	e	References
<i>ECSNe</i>							
J0737-3039A/B	1.25	1.33	6.1	0.102	22.70	0.09	1, 2
J1906+0746	1.29	1.32	1700	0.17	144.07	0.09	3
J1756-2251	1.34	1.23	5.5	0.32	28.46	0.18	4
J0453+1559	1.56	1.17	2.9	4.07	45.78	0.11	5
J1913+1102	1.62	1.27	2.1	0.21	27.29	0.09	6
J1755-2550	1.3	> 0.4	270	9.7	315.2	0.09	7
J1946+2052	1.25	1.25	4	0.09	17	0.06	8
J1757-1854	1.34	1.40	7.6	0.18	21.5	0.61	9
J0509 +3801	1.34	1.46	4.3	0.38	76.54	0.59	10
J1325-6253	1.59	0.98	1.19	1.815	22.96	0.064	11
J1018-1523	1.2	1.1	3	8.9	83	0.23	12
J1155-6529	1.4	1.27	—	3.76	79	0.26	13
J1208-5936	1.26	1.32	30	0.63	78.7	0.35	14
B1913+16	1.44	1.39	2.3	0.32	59.03	0.62	15
B1534+12	1.33	1.35	9.7	0.42	37.90	0.27	16
J1901+065	1.68	1.1	4.1	14.45	75.7	0.366	17
<i>CC SNe</i>							
J1518+4904	$1.42^{+0.51}_{-0.58}$	$1.29^{+0.58}_{-0.51}$	1.07	8.63	40.94	0.25	18
J1829+2456	1.31	1.30	1.5	1.18	41.01	0.14	19
J1930-1852	≤ 1.32	≥ 1.30	58	45.06	185.52	0.40	20
J1811-1736	< 1.64	> 0.93	9.8	18.80	104.2	0.82	21
J1753-2240		> 0.49	9.7	13.64	95.14	0.30	22
J1411+2551	< 1.62	> 0.92	5.45	0.4	0.06	0.17	23
J1759+5036	1.79	0.84	9.5	2.04	176	0.30	24
J2150+3427	< 1.67	> 0.98	49	10.6	654	0.6	25

(1)Ferdman et al. [2013], Kramer et al. [2006], Lyne et al. [2004]; (3)van Leeuwen et al. [2015]; (4)Faulkner et al. [2005], Janssen et al. [2008]; (5)Martinez et al. [2015]; (6)Lazarus et al. [2016]; (7)Ferdman et al. [2020]; (8)Ng et al. [2015]; (9)Stovall et al. [2018]; (10)Cameron et al. [2018]; (11)Lynch et al. [2018]; (12)Sengar et al. [2022]; (13)Swiggum et al. [2023]; (14)Padmanabh et al. [2023]; (15)Colom Bernadich et al. [2023]; (14)Fonseca et al. [2014]; (15)Hulse and Taylor [1975], Weisberg and Huang [2018]; (18)Swiggum et al. [2015]; (19)Corongiu et al. [2007]; (20)Keith et al. [2009]; (21)Martinez et al. [2017]; (22)Agazie et al. [2021]; (23)Wu et al. [2023]; (24)Su et al. [2024];

et al., 2024, Tauris et al., 2017, Wang et al., 2006, Wong et al., 2010]. However, the core collapse process is commonly referred to in the literature as the standard scenario. This is because it is believed to be the predominant formation mechanism for DNSs, where both components of the DNS have masses ranging from approximately $\sim 12M_\odot - 25M_\odot$ [Bhattacharya and van den Heuvel, 1991].

The Figure 3 presents the two evolutionary pathways for the formation of DNSs. The *Top – panel* of Figure 3 illustrates the formation process of the *CC* scenario. This scenario can be summarized as follows:

- (i) At the start, the system consists of two rotating main-sequence stars, designated as Star 1 and Star 2, initially having masses ranging from $12M_\odot - 25M_\odot$.
- (ii) The first NS forms in a HMXB [Li et al., 1999, Tauris et al., 2015] following first supernova event.
- (iii) The current system consists of a NS and CO or He core. Due to angular momentum and dynamical friction, there is an exchange of mass, either stably or unstable, within a

common envelope (CE) between these components [Masda et al., 2019]. This process eventually lead to the second SNe explosion of the CO or He core [van den Heuvel, 2007]. A system demonstrating considerable proper motion [Ferdman et al., 2013], might indicate its formation through *CC*. This motion could have been caused by the explosion, which imparted significant velocity to the system. Moreover, if the mass of the recycled NS is higher than that of its companion, it implies formation through the *CC*.

The *Bottom – panel* of Figure 3 illustrates the formation of DNS through the *ECSNe*. The *ECSNe* scenario was originally described by Miyaji et al. [1980] and Nomoto [1987]. In this scenario: The formation process of *ECSNe* scenario is summarized as follows:

- (i) A system is made up of two rotating $8M_\odot - 12M_\odot$ main sequence stars.
- (ii) After the first SNe, the formation of the first NS in a LMXB [Gutiérrez et al., 2005, Podsiadlowski et al., 2004];
- (iii) The current system consists of a NS and a strongly de-

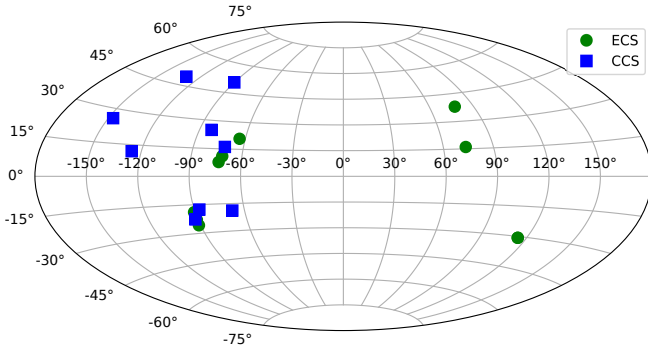


Fig. 2 The projected distribution components in our sample of DNS. Further observations in future missions (e.g., LOFAR van Haarlem et al. [2013] and FAST) may potentially result in additional discoveries of relativistic DNSs.

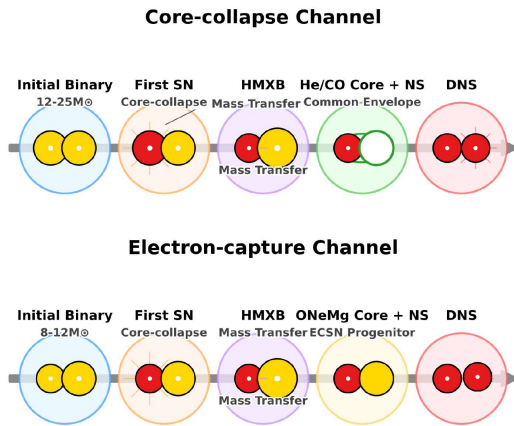


Fig. 3 The formation sketch map of DNS binaries in the Galactic disk is shown in the two panels. The *Top-panel* illustrates the *CC* scenario, where the system demonstrates considerable proper motion, indicating that its formation might be associated with a *CC* event. This motion could have arisen from the explosion, imparting significant velocity to the system. The *Bottom-panel* illustrates the *ECSNe* scenario, where the observed trend of the companion NS mass continually falling below that of the recycled NS suggests the possibility of an *ECSNe* scenario.

generate *ONeMg* core. Burning the external shell of *ONeMg* core will result in a mass increase to the Chandrasekhar limit. When ^{24}Mg and ^{24}Ne will capture electrons, the electron degeneracy pressure will be reduced [Mardini et al., 2019b], resulting in a core that reaches the nuclear matter upper limit density ($\sim 4.5 \times 10^9 \text{g/cm}^3$) in the rapid contraction process. A lower mass NS will be formed after in next SNe. The mass of the companion NS remains consistently lower than that of the recycled NS, strongly indicating the likelihood that *ECSNe* [Yang et al., 2017b].

The criteria presented in Table 1 serve to classify DNSs into distinct groups based on unique properties, show the differences in their attributes and connected to the two different formation mechanisms. This classification is based

on the unique characteristics of each mechanism. Finally, a note should be made for the Corbet diagram [Corbet, 1986] concerning the specific combination between merging and non-merging systems with different formation pathways and characteristics of the systems, *CC* and *ECSNe*. As we can see in Fig.4, that all the second-born NS binaries in DNSs forming in a *ECSNe*, are thought to experience a merging phase and then produce gravitational-wave observations, except for the system (B1534+12) [Fonseca et al., 2014]. On the other hand, systems formed via the *CC* are thought to experience a non-merging phase, except for the two systems (J0453+1559 and J1755-255) [Martinez et al., 2015]. Future detection by LIGO and VIRGO will reveal much information about these systems. This result agrees with recent work by Zhu and Ashton [2020].

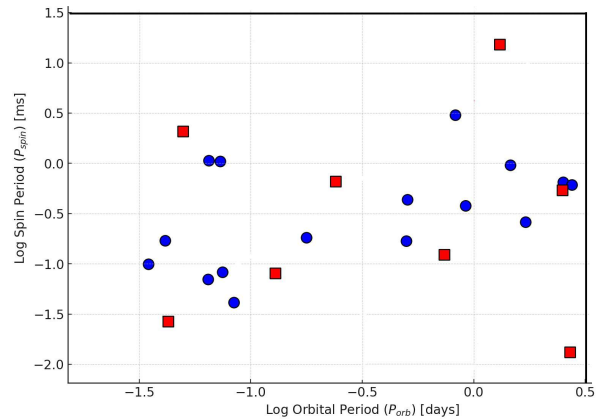


Fig. 4 The schematic depicts the approximate location of DNSs sample via the *ECSNe* (white circles) and *CC* (black squares) in the $P_{spin} - P_{orb}$ diagram.

4 Parameter analysis of DNS

This section discusses the eccentricity, orbital period, and mass of the second-born NS, to better distinguish between the DNS category.

As shown in Table 2, most companion masses are accurately measured and collected from the literature. However, the lower limit of the companion mass is given for four systems (PSR J1829+2456, J1930-1852, J1811-1736 and J1753-2240). Here, we do not consider the DNS systems residing in globular clusters (eight in total); since their characteristic properties are uniquely different from those within the Galactic disk (see Fig.5).

The masses of the 24 DNSs listed in Table 2 have been measured with high timing accuracy [Özel and Freire, 2016, Zhang et al., 2011]. It is noticeable that the masses of all recycled NSs born and spun-up by accreting matter from their companion star [Bhattacharya and van den Heuvel, 1991, Phinney and Kulkarni, 1994, van den Heuvel, 1995, Zhang and Kojima, 2006], falls within a stellar mass range

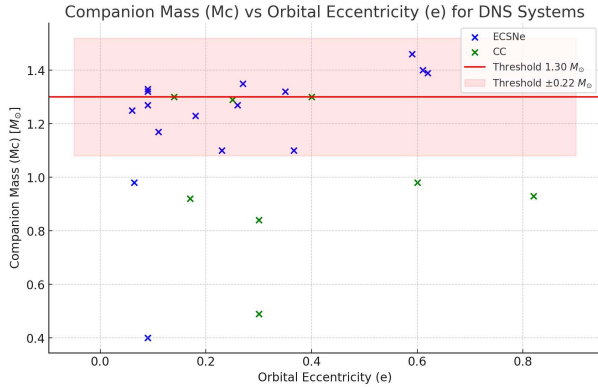


Fig. 5 The diagram plots the companion mass (M_c) against the orbital eccentricity (e) for DNSs. The red line marks the threshold at $1.30M_\odot$, with the shaded area the indicating the $\pm 0.22M_\odot$ range. This threshold visually differentiates systems likely formed via *ECSNe* and those formed through *CC* events.

of $1.29M_\odot - 1.56M_\odot$. In contrast, the mass of the second-born NS and non-recycled ranges from $1.17M_\odot$ to $1.39M_\odot$. Consequently, it is evident that the average stellar mass of non-recycled NS is higher than that of the recycled ones. The mass distribution of DNSs has a narrow deviation of approximately $0.02M_\odot$. Half of the DNSs listed in Table 1 exhibit a narrow stellar mass deviation, approximately $(1.32 \pm 0.024 M_\odot)$. Fig. 6 shows the distribution of the NS masses in DNS systems (*ECSNe* and *CC*). The histogram divided into two groups (recycled and non-recycled). Furthermore, the mass distribution of recycled NSs tends to cluster around higher values $1.48 \pm 0.025M_\odot$ reflecting the mass accretion that occurs binary evolution. In addition, this figure highlights that *ECSNe* typically produce lower mass NSs ($1.37 \pm 0.023M_\odot$), whereas *CC* are associated with higher mass systems. This distinction is further supported by the analysis *T - test*, which reveals a statistically significant difference between the mass distribution of recycled and non-recycled NS, with a confidence level of %95. The narrow mass range for DNSs suggests that the evolutionary pathways for these systems are constrained by specific physical processes and parameters during SNe, providing valuable information on the formation of NSs.

Table 1 lists the criteria for justifying whether a DNS is formed via *ECSNe* or *CC* SNe. A simple statistical overview of key property ranges for DNS systems is presented. The categorization of DNSs into two groups was performed on the basis of the specific criteria that reflect the unique characteristics associated with the two distinct formation mechanisms.

The dichotomy in the magnetic field strengths between NSs formed via *ECSNe* and *CC* originates from their fundamentally distinct explosion mechanisms and post-formation evolution paths [Taani et al., 2012b]. *ECSNe*, which arise from low-mass progenitors, produce relatively symmetric,

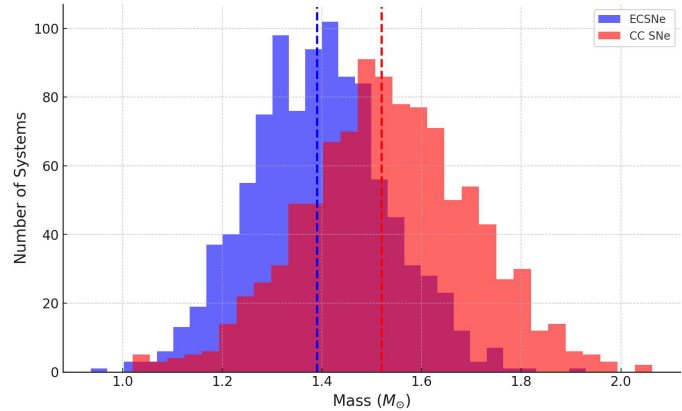


Fig. 6 The histogram illustrates the mass distribution of the DNS systems formed via *ECSNe* (with a mean mass of $1.39M_\odot$) and *CC* (with a mean mass of $1.52M_\odot$). The dashed vertical lines indicate the average mass of each group.

This visual representation highlights the difference in mass between the two formation scenarios, providing the insight into characteristics and evolutionary processes of these binary systems.

low-energy explosions that preserve the magnetic field configuration of the progenitor, typically resulting in weaker surfaces fields ($\sim 10^{9-10}$ G; e.g., Zhang et al. 2011). In contrast, *CC* involve violent, asymmetric explosions, where extreme turbulence and convective dynamos during collapse and amplify surface fields to $\sim 10^{11-13}$ G (e.g., Janka [2012], Jones and et al. [2019]). Furthermore, recycled NSs, which often form in close binaries, can accrete substantial mass of $\sim 0.1M_\odot - 0.2M_\odot$ Zhang et al. [2011], leading to longer lifespan and magnetic field decay due to accretion-driven burial, as well as faster spin periods (Taani et al. 2012b). In contrast, non-recycled NSs formed directly from *CC* events typically retain strong magnetic fields ($\sim 10^{12}$ G) and experience shorter spin-down timescales (van den Heuvel 2017). This combination of explosion dynamics and accretion history fundamentally shapes the observed magnetic field distributions among NSs.

4.1 DNS mass distribution and T-test

We used statistical *T - test* to quantitatively evaluate our sample and compare the mean values of the two groups of DNS components. This method involves defining the parameter t to determine if the means (averages) of two sample groups with different types of companions are significantly different [John, 2006]:

$$t = \frac{\bar{X}_1 - \bar{X}_2}{S_p \sqrt{2/n_1 + 2/n_2}}, \quad (1)$$

where \bar{X}_1 and \bar{X}_2 are the averages of two groups, ($n_1 = 16$), ($n_2 = 8$) are the number of samples in each group that defines

the degree of freedom for this test ($d = 2n - 2 = 16$). The pooled standard deviation is denoted by the parameter S_p ,

$$S_p = \sqrt{\frac{S_{X_1}^2 + S_{X_2}^2}{2}}, \quad (2)$$

where $S_{X_1}^2$ and $S_{X_2}^2$ are the unbiased estimators of the variances of two groups.

Based on the updated data from the two DNS mass groups, we calculated the t-parameter, yielding $t=2.02$. Our analysis further reveals that for the significance levels of 95% and 99%, the critical t-values are $t_{0.05(d=24)} = 2.075 < t < t_{0.05(d=24)} = 2.075$, and $t_{0.01(d=24)} = 2.82 < t < t_{0.01(d=24)} = 2.82$. Since our calculated t-value falls below the 95% threshold, the results indicate that the difference in mass distributions between the two groups (recycled NSs and their companions) suggests a potential trend where the stellar mass of the recycled NSs may tend to be higher than that of the non-recycled companions (see Table 2).

When comparing the mass distribution of DNSs with that of MSPs, we find that the deviation of the DNS mass distribution is approximately $\sim 0.02 M_\odot$, which is roughly ten times lower than that of the MSPs (approximately $\sim 0.2 M_\odot$) as reported by [Zhang et al., 2011]. The recent measurement of NS mass statistics, including around ~ 70 , indicates that all the measured NS masses are distributed within a broader range, approximately $[\sim 1 M_\odot - 2 M_\odot]$ [Özel and Freire, 2016, Zhang et al., 2011]. Consequently, we can conclude that the specific evolutionary history of DNSs significantly contributes to their mass formation, and there must be a mechanism constraining the birth mass of DNSs to a narrower range. The observed mass range reflects both the initial mass distribution and the impact of the accretion phase [Ferdman et al. [2020], Podsiadlowski et al. [2004].

Fig. 7 presents the fitting curves based on condition ($e \times P_{orb} < 0.05$), which serves as a boundary between DNS systems formed via *ECSNe* and *CC*. The region below the line ($e \times P_{orb} < 0.05$) corresponds to systems with lower eccentricities and shorter orbital periods, indicative of formation through *ECSNe*, where SNe imparted minimal kicks to the systems. On the other hand, the region above the line ($e \times P_{orb} > 0.05$) represents systems with higher eccentricities and longer orbital periods, characteristics of formation through *CC* mechanisms, where larger kicks are expected. Several systems deviate from the curves' predictions, indicating the presence of additional factors such as significant mass transfer or unique evolutionary pathways. More observations are needed for further investigation [Ding et al., 2024, Kramer et al., 2021]

To further investigate the evolution history and mass formation conditions of DNS, we compare DNSs with MSPs using the magnetic field versus spin period (B-P) diagram, as shown in Figure 8. Two DNS systems, J1906+0746 ($B \sim 17 \times 10^{12}$ G, $P_s = 144$ ms) and J0737-3039B ($B \sim 16 \times 10^{12}$ G, $P_s = 773$ ms) appear above the spin-up line, which is unusual for DNSs. These systems exhibit spin periods that

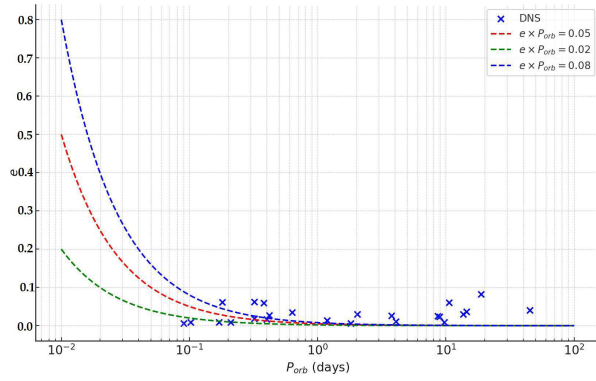


Fig. 7 The diagram plots the eccentricity (e) against orbital period for the DNSs. The colored curves represent the condition $e \times P_{orb} = 0.05$ (with P_{orb} in unit of days). This condition separates the DNS samples into two regions based on their formation pathways and system characteristics: *ECSNe* (where $e \times P_{orb} < 0.05$) and *CC* (where $e \times P_{orb} > 0.05$), respectively.

are too long for their magnetic fields according to spin-up theory, suggesting that they behave differently from typical recycled pulsars, which generally fall along the spin-up line. [Yang et al., 2017b], conducted an in-depth analysis of these two DNSs and concluded that both systems share a similar origin and evolutionary process, likely involving e-capture for the formation of the second-born NS. Furthermore, their companions are expected to be a long-lived recycled-pulsars.

However, we excluded PSR J1807-2500B and J1411 + 2551 because of the high uncertainty in their magnetic field.

The evolutionary history of DNSs and MSPs is evident in their distinct positions on the B-P diagram. MSPs generally accumulate around $\geq 0.1 M_\odot - 0.2 M_\odot$ while DNSs absorb approximately $\sim 0.001 M_\odot - 0.01 M_\odot$ from their companions [Bhattacharya and van den Heuvel, 1991, Pan et al., 2015, Zhang and Kojima, 2006]. Furthermore, MSPs are the result of LMXBs (e.g., companion mass of $\sim 1 M_\odot - 2 M_\odot$), whereas DNSs are primarily involved in HMXBs (e.g., companion mass of $8 M_\odot - 10 M_\odot$ for electron capture [Nomoto, 1987] and $10 - 25 M_\odot$ for the SN explosion [Dewi et al., 2006]). Generally, the LMXB is very long lived at a time scale of a dozen billion years, so the MSP has a sufficient time to accumulate matter from the companion. In addition, the less massive companion star holds a small size, it is weakly influenced by the primary star when compared to the case of HMXB. As a result, the mass distribution of the MSPs inherits that of the isolated NSs by SNe explosions, by adding the accretion mass of $\sim 0.1 M_\odot - 0.2 M_\odot$. Therefore, the distribution of MSP masses is very broad, from $\sim 1.2 M_\odot$ to $\sim > 2.0 M_\odot$ [Özel and Freire, 2016, Zhang et al., 2011].

We conducted an investigation of statistically significant similarities among these DNSs by employing unsupervised

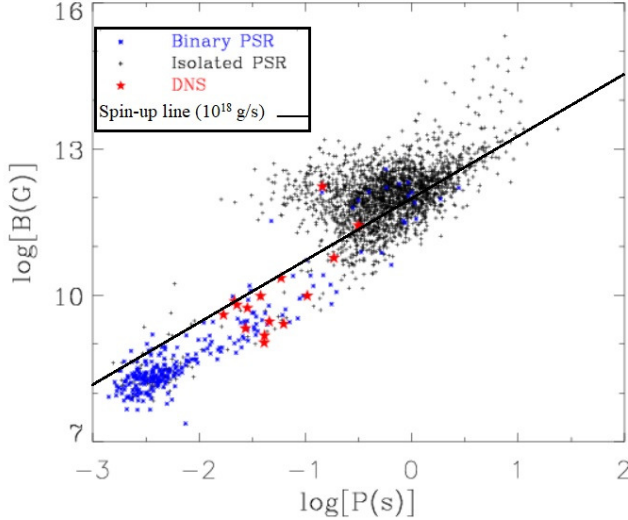


Fig. 8 The magnetic-field versus spin-period diagram for DNSs is shown. The solid lines represent the spin-up lines with the accretion rate of 10^{18} g/s. The isolated pulsars, binary pulsars and DNSs are labeled with dots, pentagram and stars, respectively (for details see [Bhattacharya and van den Heuvel, 1991]). The pulsar data in this figure are taken from ATNF pulsar catalogue [Manchester et al., 2005].

clustering algorithms, specifically HDBSCAN. This analysis would help us to understand whether these stars experienced similar evolution histories. Our clustering analysis focused on crucial parameters: Mass, orbital period and magnetic field parameters. To facilitate this analysis, normalization of these variables was necessary. We achieved this normalization using the `Astropy.stats.biweight_location()` and `astropy.stats.biweight_scale()` routines¹. As a result, we identify the DNSs distribution's central position as the following formula:

$$\zeta_{biloc} = M + \frac{\sum_{|u_i| < 1} (x_i - M)(1 - u_i^2)^2}{\sum_{|u_i| < 1} (1 - u_i^2)^2}$$

We also compute the standard deviation of DNSs distribution using the following formula:

$$\zeta_{biscl} = \sqrt{n} \frac{\sqrt{\sum_{|u_i| < 1} (x_i - M)^2 (1 - u_i^2)^4}}{|\sum_{|u_i| < 1} (1 - u_i^2)(1 - 5u_i^2)|}$$

After normalizing the selected parameters, we utilized specific HDBSCAN parameters: `min_cluster_size = 5`, `min_samples = 5`, `cluster_selection_method = leaf`, `prediction_data = True`, and minimum confidence set to 20%. These combinations of parameters led to the identification of two clusters. In Figure 9, we can observe the tagged stars in each of the chosen parameters spaces. Filled pointing-up triangle and square symbols denote the first and second cluster, respectively. Asterisk symbol represent Outliers DNSs; differs significantly from other observations. By examining the true cluster labels (i.e., *ECSNe* and *CC*) of the two groups, we found that the *ECSNe* and *CC* source are likely to be well separated in 3D-space

¹ For a detailed description of the `biweight_location()` algorithm visit: https://docs.astropy.org/en/stable/api/astropy.stats.biweight_location.html

(mass, orbital period, and magnetic field). Finally, considering the strong correlations and degeneracy between parameters that affect evolutionary paths of DNS formation, the application of HDBSCAN would require various choices to investigate to understand how the assumptions would affect the results.

5 Discussions and Conclusions

It is interesting to study DNS masses and compare them with MSP masses, as the nuclear matter compositions are different. The mass estimation of NSs with different mass-transfer histories is shown in a B-P diagram. As a result, the mass distribution of the MSPs will have a distribution similar to that of the isolated NSs. Furthermore, if further mass accretion exceeds the range of $0.1M_{\odot} - 0.2M_{\odot}$, it is possible to explain the heavy MSPs distributed in a broader regime ($\sim 1.2M_{\odot} - 2.0M_{\odot}$) than DNSs. This includes nuclear matter classifications, *r*-process nucleosynthesis of elements [Almusleh et al., 2021, Mardini et al., 2019b,c, 2020], gravitational waves, and neutrino emission between DNS and MSPs [Mardini et al., 2019a].

We applied the *T-test* to statistically evaluate the differences in mean mass distribution between recycled and non-recycled components within the DNSs. The calculated means and standard deviations for the two samples are $1.370 \pm 0.023M_{\odot}$ and $1.48 \pm 0.025M_{\odot}$ respectively. A distinction of approximately ($\Delta M = 0.1 \pm 0.034M_{\odot}$) with a deviation of approximately 3 sigma was observed. The application of HDBSCAN in our analysis enhances the robustness of our clustering approach, efficiently identifying the formation and evolution of DNSs. This method reveals significant patterns and relationships in the diverse population of DNSs.

An analysis of companion masses revealed a crucial threshold round $1.30M_{\odot} \pm 0.22M_{\odot}$, playing a significant role in the evolutionary process of DNSs. Below this threshold, the formation via the *ECSNe* is represented by merging objects characterized by minimal orbital eccentricity and transverse velocity. Note that PSR J1906+0746 is considered a strong candidate for formation through *ECSNe*, even with a companion mass of $1.32M_{\odot}$.

On the other hand, the *CC* model, involving non-merging objects requires a companion mass greater than $1.30M_{\odot}$. Our analysis suggests that in several systems, the second-born NS likely originated from *ECSNe*, raising the likelihood of a low kick velocity. This result would leave the NS provisionally bound post-explosion with low eccentricity. This mechanism can also produce a low-mass NS.

Finally, the conclusions of the present investigation are considered an initial effort to study the physical parameters and distributions of DNSs. It is also a promising step toward understanding the formation and evolution processes of these systems. We strongly recommend further observations, using more sensitive instruments on future missions

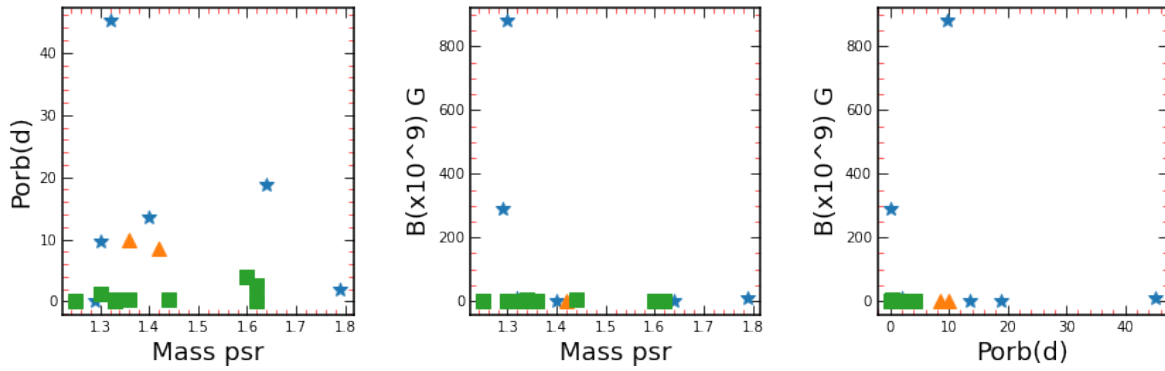


Fig. 9 Left panel illustrates the two identified clusters in the M , P_{orb} space. The middle panel displays the two identified clusters in the M and B space. The right panel exhibits the two identified clusters in the P_{orb} and B space. Asterisk symbols represent stars that do not fall into any cluster (Noise).

(e.g., advanced Virgo detector², Einstein Telescope or Cosmic Explorer³, LOFAR⁴, and FAST⁵), which might lead to more discoveries of relativistic DNSs. Furthermore, the planned SKA⁶ is expected to find more DNSs and provide important clues about the nuclear matter compositions of these pulsars.

Acknowledgements. We are grateful to Y. Yang for his suggestions that allowed us to improve the clarity of the original version. Special thanks to B.-S. Liu for helping with some figures.

References

- B. P. Abbott, R. Abbott, T. D. Abbott, and et al. GW151226: Observation of Gravitational Waves from a 22-Solar-Mass Binary Black Hole Coalescence. *Phys. Rev. Lett.*, 116(24):241103, 2016.
- B. P. Abbott, R. Abbott, T. D. Abbott, and et al. GW170814: A Three-Detector Observation of Gravitational Waves from a Binary Black Hole Coalescence. *Phys. Rev. Lett.*, 119(14):141101, 2017a.
- B. P. Abbott, R. Abbott, T. D. Abbott, and et al. GW170817: Observation of Gravitational Waves from a Binary Neutron Star Inspiral. *Phys. Rev. Lett.*, 119(16):161101, 2017b.
- B. P. Abbott, R. Abbott, T. D. Abbott, and et al. GW190425: Observation of a Compact Binary Coalescence with Total Mass $\sim 3.4 M_{\odot}$. *ApJ*, 892(1):L3, 2020.
- R. Abbott and et al. GWTC-3: Compact Binary Coalescences Observed by LIGO and Virgo during the Second Part of the Third Observing Run. *Physical Review X*, 13(4):041039, 2023.
- M. Abu-Saleem and A. Taani. Retraction and folding on the hyperbolic black hole. *AIP Advances*, 11(1):015309, 2021a.
- M. Abu-Saleem and A. Taani. Geometric transformations on a topological black hole and their applications. *Chinese Journal of Physics*, 74:53–59, 2021b.
- F. Acernese and et al. Virgo detector characterization and data quality: results from the O3 run. *Classical and Quantum Gravity*, 40(18):185006, 2023.
- G. Y. Agazie, M. G. Mingyar, M. A. McLaughlin, and et al. The Green Bank Northern Celestial Cap Pulsar Survey. VI. Discovery and Timing of PSR J1759+5036: A Double Neutron Star Binary Pulsar. *ApJ*, 922(1):35, 2021.
- H. Aljboor and A. Taani. Speckle-interferometric Study of Close Visual Binary System HIP 11253 (HD 14874) using Gaia (DR2 and EDR3). *Research in Astronomy and Astrophysics*, 23(7): 075018, 2023.
- N. A. Almusleh, A. Taani, S. Özdemir, M. Rah, M. A. Al-Wardat, G. Zhao, and M. K. Mardini. Metal-poor stars observed with the automated planet finder telescope. III. CEMP-no stars are the descendant of population III stars. *Astronomische Nachrichten*, 342(4):625–632, 2021.
- J. J. Andrews, W. M. Farr, V. Kalogera, and B. Willems. Evolutionary Channels for the Formation of Double Neutron Stars. *ApJ*, 801(1):32, 2015.
- D. Bhattacharya and E. P. J. van den Heuvel. Formation and evolution of binary and millisecond radio pulsars. *Journal of Astrophysics and Astronomy*, 203(1-2):1–124, 1991.
- S. e. a. Borhanian. Listening to the Universe with next generation ground-based gravitational-wave detectors. *Phys. Rev. D*, 110(8):083040, 2024.
- M. Burgay, N. D’Amico, A. Possenti, and et al. An increased estimate of the merger rate of double neutron stars from observations of a highly relativistic system. *Nature*, 426(6966): 531–533, 2003.
- M. Burgay, D. Perrodin, and A. Possenti. General Relativity Measurements from Pulsars. In T. M. Belloni, M. Méndez, and C. Zhang, editors, *Timing Neutron Stars: Pulsations, Oscillations and Explosions*, volume 461 of *Astrophysics and Space Science Library*, pages 53–95, 2021.
- A. D. Cameron, D. J. Champion, M. Kramer, and et al. The High Time Resolution Universe Pulsar Survey - XIII. PSR J1757-1854, the most accelerated binary pulsar. *MNRAS*, 475(1):L57–L61, 2018.
- D. J. Champion, D. R. Lorimer, M. A. McLaughlin, J. M. Cordes, Z. Arzoumanian, J. M. Weisberg, and J. H. Taylor. PSR J1829+2456: a relativistic binary pulsar. *MNRAS*, 350(4):L61–L65, 2004.

² <https://www.virgo-gw.eu/>

³ <https://www.et-gw.eu/>

⁴ <https://www.astron.nl/lofar2-0-newsletter/lofar-development-newsletter-december-2024/>

⁵ <https://fast.bao.ac.cn/>

⁶ <https://www.skao.int/en>

- D. Chattopadhyay, S. Stevenson, J. R. Hurley, L. J. Rossi, and C. Flynn. Modelling double neutron stars: radio and gravitational waves. *Monthly Notices of the Royal Astronomical Society*, 494(2):1587–1610, 2020. ISSN 0035-8711.
- Z. Cheng, C. Zhang, and A. Taani. Monte Carlo Simulation of Neutron Star Masses. In *International Journal of Modern Physics Conference Series*, volume 23 of *International Journal of Modern Physics Conference Series*, pages 157–160, 2013.
- J. A. Clark, A. Bauswein, N. Stergioulas, and D. Shoemaker. Observing gravitational waves from the post-merger phase of binary neutron star coalescence. *Classical and Quantum Gravity*, 33(8):085003, 2016.
- M. Colom Bernadich, V. Balakrishnan, Barr, and E. et al. The MPIfR-MeerKAT Galactic Plane Survey. II. The eccentric double neutron star system PSR J1208–5936 and a neutron star merger rate update. *A&A*, 678:A187, 2023.
- R. H. D. Corbet. The three types of high-mass X-ray pulsator. *MNRAS*, 220:1047–1056, 1986.
- A. Corongiu, M. Kramer, B. W. Stappers, A. G. Lyne, A. Jessner, A. Possenti, N. D’Amico, and O. Löhmer. The binary pulsar PSR J1811-1736: evidence of a low amplitude supernova kick. *A&A*, 462(2):703–709, 2007.
- Z. Dai, P. Szkody, A. Taani, P. M. Garnavich, and M. Kennedy. Quiescent photometric modulations of two low-inclination cataclysmic variables KZ Geminorum and TW Virginis. *A&A*, 606:A45, 2017.
- J. D. M. Dewi, P. Podsiadlowski, and A. Sena. Double-core evolution and the formation of neutron star binaries with compact companions. *MNRAS*, 368(4):1742–1748, 2006.
- H. Ding, A. T. Deller, J. K. Swiggum, R. S. Lynch, S. Chatterjee, and T. M. Tauris. VLBA Astrometry of the Galactic Double Neutron Stars PSR J0509+3801 and PSR J1930–1852: A Preliminary Transverse Velocity Distribution of Double Neutron Stars and its Implications. *ApJ*, 970(1):90, 2024.
- A. J. Faulkner, M. Kramer, A. G. Lyne, and et al. PSR J1756-2251: A New Relativistic Double Neutron Star System. *ApJ*, 618(2):L119–L122, 2005.
- R. D. Ferdman, I. H. Stairs, M. Kramer, and et al. The Double Pulsar: Evidence for Neutron Star Formation without an Iron Core-collapse Supernova. *ApJ*, 767(1):85, 2013.
- R. D. Ferdman, I. H. Stairs, M. Kramer, and et al. PSR J1756-2251: a pulsar with a low-mass neutron star companion. *MNRAS*, 443(3):2183–2196, 2014.
- R. D. Ferdman, P. C. C. Freire, B. B. P. Perera, and et al. Asymmetric mass ratios for bright double neutron-star mergers. *Nature*, 583(7815):211–214, 2020.
- E. Fonseca, I. H. Stairs, and S. E. Thorsett. A Comprehensive Study of Relativistic Gravity Using PSR B1534+12. *ApJ*, 787(1):82, 2014.
- S. Galadage, C. Adamcewicz, X.-J. Zhu, S. Stevenson, and E. Thrane. Heavy Double Neutron Stars: Birth, Midlife, and Death. *ApJ*, 909(2):L19, 2021.
- J. Gutiérrez, R. Canal, and E. García-Berro. The gravitational collapse of One electron-degenerate cores and white dwarfs: The role of ^{24}Mg and ^{12}C revisited. *A&A*, 435(1):231–237, 2005.
- R. A. Hulse and J. H. Taylor. Discovery of a pulsar in a binary system. *ApJ*, 195:L51–L53, 1975.
- H.-T. Janka. Explosion Mechanisms of Core-Collapse Supernovae. *Annual Review of Nuclear and Particle Science*, 62(1):407–451, 2012.
- G. H. Janssen, B. W. Stappers, M. Kramer, D. J. Nice, A. Jessner, I. Cognard, and M. B. Purver. Multi-telescope timing of PSR J1518+4904. *A&A*, 490(2):753–761, 2008.
- A. R. John. *Mathematical Statistics and Data Analysis, Third Edition, Duxbury Advanced*. Princeton University, Cambridge, Massachusetts, 2006.
- S. Jones and et al. Remnants and ejecta of thermonuclear electron-capture supernovae. Constraining oxygen-neon deflagrations in high-density white dwarfs. *A&A*, 622:A74, 2019.
- V. Kalogera, B. S. Sathyaprakash, M. Bailes, and et al. The Next Generation Global Gravitational Wave Observatory: The Science Book. *arXiv e-prints*, art. arXiv:2111.06990, 2021.
- L. Kasian. Timing and Precession of the Young, Relativistic Binary Pulsar PSR J1906+0746. In C. Bassa, Z. Wang, A. Cumming, and V. M. Kaspi, editors, *40 Years of Pulsars: Millisecond Pulsars, Magnetars and More*, volume 983 of *American Institute of Physics Conference Series*, pages 485–487, 2008.
- M. J. Keith, M. Kramer, A. G. Lyne, R. P. Eatough, I. H. Stairs, A. Possenti, F. Camilo, and R. N. Manchester. PSR J1753-2240: a mildly recycled pulsar in an eccentric binary system. *MNRAS*, 393(2):623–627, 2009.
- C. Kim, B. B. P. Perera, and M. A. McLaughlin. Implications of PSR J0737-3039B for the Galactic NS-NS binary merger rate. *MNRAS*, 448(1):928–938, 2015.
- A. E. Koloniari, E. C. Koursoumpa, P. Nousi, P. Lampropoulos, N. Passalis, A. Tefas, and N. Stergioulas. New gravitational wave discoveries enabled by machine learning. *Machine Learning: Science and Technology*, 6(1):015054, 2025.
- M. Kramer, I. H. Stairs, R. N. Manchester, and et al. Tests of General Relativity from Timing the Double Pulsar. *Science*, 314(5796):97–102, 2006.
- M. Kramer, I. H. Stairs, R. N. Manchester, and et al. Strong-Field Gravity Tests with the Double Pulsar. *Physical Review X*, 11(4):041050, 2021.
- M. Kramer, I. H. Stairs, R. N. Manchester, and et al. Strong-field gravity tests with the double pulsar. *Phys. Rev. X*, 11:041050, 2021.
- M. U. Kruckow, T. M. Tauris, N. Langer, M. Kramer, and R. G. Izzard. Progenitors of gravitational wave mergers: binary evolution with the stellar grid-based code COMBINE. *MNRAS*, 481(2):1908–1949, 2018.
- P. D. Lasky. Gravitational waves from neutron stars: A review. *Publications of the Astronomical Society of Australia*, 32:e034, 2015.
- P. Lazarus, P. C. C. Freire, B. Allen, and et al. Einstein@Home Discovery of a Double Neutron Star Binary in the PALFA Survey. *ApJ*, 831(2):150, 2016.
- X. D. Li, I. Bombaci, M. Dey, J. Dey, and E. P. J. van den Heuvel. Is SAX J1808.4-3658 a Strange Star? *Phys. Rev. Lett.*, 83(19):3776–3779, 1999.
- R. S. Lynch, J. K. Swiggum, V. I. Kondratiev, and et al. The Green Bank North Celestial Cap Pulsar Survey. III. 45 New Pulsar Timing Solutions. *ApJ*, 859(2):93, 2018.
- A. G. Lyne, M. Burgay, M. Kramer, and et al. A Double-Pulsar System: A Rare Laboratory for Relativistic Gravity and Plasma Physics. *Science*, 303(5661):1153–1157, 2004.
- R. N. Manchester, G. B. Hobbs, A. Teoh, and M. Hobbs. The Australia Telescope National Facility Pulsar Catalogue. *AJ*, 129(4):1993–2006, 2005.
- M. K. Mardini, N. Ershiadat, M. A. Al-Wardat, A. A. Taani, S. Özdemir, H. Al-Naimiy, and A. Khasawneh. The Nucleosyn-

- thesis and Reaction Rates of Fluorine ^{19}F in the Sun. In *Journal of Physics Conference Series*, volume 1258 of *Journal of Physics Conference Series*, page 012024, 2019a.
- M. K. Mardini, H. Li, V. M. Placco, S. Alexeeva, D. Carollo, A. Taani, I. Ablimit, L. Wang, and G. Zhao. Metal-poor Stars Observed with the Automated Planet Finder Telescope. I. Discovery of Five Carbon-enhanced Metal-poor Stars from LAMOST. *ApJ*, (2):89, Apr 2019b.
- M. K. Mardini, V. M. Placco, A. Taani, H. Li, and G. Zhao. Metal-poor Stars Observed with the Automated Planet Finder Telescope. II. Chemodynamical Analysis of Six Low-metallicity Stars in the Halo System of the Milky Way. *ApJ*, (1):27, Sep 2019c.
- M. K. Mardini, V. M. Placco, and et al. Cosmological Insights into the Early Accretion of r-process-enhanced Stars. I. A Comprehensive Chemodynamical Analysis of LAMOST J1109+0754. *ApJ*, 903(2):88, 2020.
- J. G. Martinez, K. Stovall, P. C. C. Freire, and et al. Pulsar J0453+1559: A Double Neutron Star System with a Large Mass Asymmetry. *ApJ*, 812(2):143, 2015.
- J. G. Martinez, K. Stovall, P. C. C. Freire, and et al. Pulsar J1411+2551: A Low-mass Double Neutron Star System. *ApJ*, 851(2):L29, 2017.
- S. G. Masda, J. A. Docobo, A. M. Hussein, M. K. Mardini, H. A. Al-Ameryeen, P. P. Campo, A. R. Khan, and J. M. Pathan. Physical and Dynamical Parameters of the Triple Stellar System: HIP 109951. *Astrophysical Bulletin*, 74(4):464–474, 2019.
- D. McClelland, H. Lueck, R. Adhikari, and et al. 3G R&D: R&D for the Next Generation of Ground-based Gravitational-wave Detectors. *arXiv e-prints*, art. arXiv:2111.06991, 2021.
- M. C. Miller and N. Yunes. The new frontier of gravitational waves. *Nature*, 568(7753):469–476, 2019.
- S. Miyaji, K. Nomoto, K. Yokoi, and D. Sugimoto. Supernova triggered by electron captures. *PASJ*, 32:303–329, 1980.
- C. Ng, D. J. Champion, M. Bailes, and et al. The High Time Resolution Universe Pulsar Survey - XII. Galactic plane acceleration search and the discovery of 60 pulsars. *MNRAS*, 450(3):2922–2947, 2015.
- A. H. Nitz, S. Kumar, Y.-F. Wang, S. Kastha, S. Wu, M. Schäfer, R. Dhurkunde, and C. D. Capano. 4-OGC: Catalog of Gravitational Waves from Compact Binary Mergers. *ApJ*, 946(2):59, 2023.
- K. Nomoto. Evolution of 8–10 M_{sun} Stars toward Electron Capture Supernovae. II. Collapse of an O + NE + MG Core. *ApJ*, 322:206, 1987.
- F. Özel and P. Freire. Masses, Radii, and the Equation of State of Neutron Stars. *ARA&A*, 54:401–440, 2016.
- P. V. Padmanabh, E. D. Barr, S. S. Sridhar, and et al. The MPIfR-MeerKAT Galactic Plane Survey - I. System set-up and early results. *MNRAS*, 524(1):1291–1315, 2023.
- Y. Y. Pan, L. M. Song, C. M. Zhang, and Y. Q. Guo. The simulation of the magnetic field and spin period evolution of accreting neutron stars. *Astronomische Nachrichten*, 336(4):370–377, 2015.
- E. S. Phinney and S. R. Kulkarni. Binary and Millisecond Pulsars. *ARA&A*, 32:591–639, 1994.
- P. Podsiadlowski, N. Langer, A. J. T. Poelarends, S. Rappaport, A. Heger, and E. Pfahl. The Effects of Binary Evolution on the Dynamics of Core Collapse and Neutron Star Kicks. *ApJ*, 612(2):1044–1051, 2004.
- P. Podsiadlowski, J. D. M. Dewi, P. Lesaffre, J. C. Miller, W. G. Newton, and J. R. Stone. The double pulsar J0737-3039: testing the neutron star equation of state. *MNRAS*, 361(4):1243–1249, 2005.
- R. Sengar, V. Balakrishnan, and et al. The High Time Resolution Universe Pulsar Survey - XVII. PSR J1325-6253, a low eccentricity double neutron star system from an ultra-stripped supernova. *MNRAS*, 512(4):5782–5792, 2022.
- Y. Shao and X.-D. Li. On the Role of Supernova Kicks in the Formation of Galactic Double Neutron Star Systems. *ApJ*, 867(2):124, 2018.
- B. J. Shappee, J. D. Simon, M. R. Drout, and et al. Early spectra of the gravitational wave source GW170817: Evolution of a neutron star merger. *Science*, 358(6370):1574–1578, 2017.
- I. H. Stairs, S. E. Thorsett, R. J. Dewey, M. Kramer, and C. A. McPhee. The formation of the double pulsar PSR J0737-3039A/B. *MNRAS*, 373(1):L50–L54, 2006.
- K. Stovall, P. C. C. Freire, S. Chatterjee, and et al. PALFA Discovery of a Highly Relativistic Double Neutron Star Binary. *ApJ*, 854(2):L22, 2018.
- W. Q. Su, J. L. Han, and Z. L. e. a. Yang. The FAST Galactic Plane Pulsar Snapshot Survey - V. PSR J1901+0658 in a double neutron star system. *MNRAS*, 530(2):1506–1511, 2024.
- J. K. Swiggum, R. Rosen, M. A. McLaughlin, and et al. PSR J1930-1852: a Pulsar in the Widest Known Orbit around Another Neutron Star. *ApJ*, 805(2):156, 2015.
- J. K. Swiggum, Z. Pleunis, E. Parent, and et al. The Green Bank North Celestial Cap Survey. VII. 12 New Pulsar Timing Solutions. *ApJ*, 944(2):154, 2023.
- A. Taani. Systematic comparison of initial velocities for neutron stars in different models. *Research in Astronomy and Astrophysics*, 16(7):101, 2016.
- A. Taani. Characterizing the Regular Orbits of Binary Pulsars: An Initial Prospection Study. *Galaxies*, 11(2):44, 2023.
- A. Taani and A. Khasawneh. Probing the accretion induced collapse of white dwarfs in millisecond pulsars. In *Journal of Physics Conference Series*, volume 869 of *Journal of Physics Conference Series*, page 012090, 2017.
- A. Taani and J. C. Vallejo. Dynamical Monte Carlo Simulations of 3-D Galactic Systems in Axisymmetric and Triaxial Potentials. *PASA*, 34:e024, 2017.
- A. Taani, L. Naso, Y. Wei, C. Zhang, and Y. Zhao. Modeling the spatial distribution of neutron stars in the Galaxy. *Ap&SS*, 341(2):601–609, 2012a.
- A. Taani, C. Zhang, M. Al-Wardat, and Y. Zhao. Investigation of some physical properties of accretion induced collapse in producing millisecond pulsars. *Ap&SS*, 340(1):147–153, 2012b.
- A. Taani, S. Karino, L. Song, C. Zhang, and S. Chaty. Determination of wind-fed model parameters of neutron stars in high-mass X-ray binaries. *PASA*, 39:e040, 2022a.
- A. Taani, J. C. Vallejo, and M. Abu-Saleem. Assessing the complexity of orbital parameters after asymmetric kick in binary pulsars. *Journal of High Energy Astrophysics*, 35:83–90, 2022b.
- T. M. Tauris and E. P. J. van den Heuvel. *Physics of Binary Star Evolution. From Stars to X-ray Binaries and Gravitational Wave Sources*. 2023.
- T. M. Tauris and E. P. J. van den Heuvel. Physics of binary star evolution – from stars to x-ray binaries and gravitational wave sources, 2023. URL <https://arxiv.org/abs/2305.09388>.
- T. M. Tauris, N. Langer, and P. Podsiadlowski. Ultra-stripped supernovae: progenitors and fate. *MNRAS*, 451(2):2123–2144, 2015.

- T. M. Tauris, M. Kramer, P. C. C. Freire, and et al. Formation of Double Neutron Star Systems. *ApJ*, (2):170, Sept. 2017.
- E. P. J. van den Heuvel. Scenarios for the formation of binary and millisecond pulsars - A critical assessment. *Journal of Astrophysics and Astronomy*, 16:255–288, 1995.
- E. P. J. van den Heuvel. Double Neutron Stars: Evidence For Two Different Neutron-Star Formation Mechanisms. In T. di Salvo, G. L. Israel, L. Piersant, L. Burderi, G. Matt, A. Tornambe, and M. T. Menna, editors, *The Multicolored Landscape of Compact Objects and Their Explosive Origins*, volume 924 of *American Institute of Physics Conference Series*, pages 598–606, 2007.
- E. P. J. van den Heuvel. High space velocities of single radio pulsars versus low orbital eccentricities and masses of double neutron stars: Evidence for two different neutron star formation mechanisms. *NewAR*, 54(3-6):140–144, 2010.
- E. P. J. van den Heuvel. Formation of Double Neutron Stars, Millisecond Pulsars and Double Black Holes. *Journal of Astrophysics and Astronomy*, 38(3):45, 2017.
- M. P. van Haarlem, M. W. Wise, A. W. Gunst, and et al. LOFAR: The LOw-Frequency ARray. *A&A*, 556:A2, 2013.
- J. van Leeuwen, L. Kasian, I. H. Stairs, and et al. The Binary Companion of Young, Relativistic Pulsar J1906+0746. *ApJ*, 798(2):118, 2015.
- C. Wang, D. Lai, and J. L. Han. Neutron Star Kicks in Isolated and Binary Pulsars: Observational Constraints and Implications for Kick Mechanisms. *ApJ*, 639(2):1007–1017, 2006.
- J. M. Weisberg and Y. Huang. Relativistic Measurements from Timing the Binary Pulsar PSR B1913+16. *ApJ*, 829(1):55, 2016.
- J. M. Weisberg, D. J. Nice, and J. H. Taylor. Timing Measurements of the Relativistic Binary Pulsar PSR B1913+16. *ApJ*, 722(2):1030–1034, 2010.
- N. Wex. Neutron Stars as Probes for General Relativity and Gravitational Waves. In A. W. Alsabti and P. Murdin, editors, *Handbook of Supernovae*, page 1447. Springer International Publishing, 2017.
- T.-W. Wong, B. Willems, and V. Kalogera. Constraints on Natal Kicks in Galactic Double Neutron Star Systems. *ApJ*, 721(2):1689–1701, 2010.
- Q. D. Wu, N. Wang, J. P. Yuan, and et al. PSR J2150+3427: A Possible Double Neutron Star System. *ApJ*, 958(1):L17, 2023.
- Y.-Y. Yang, L. Chen, R.-F. Linghu, L.-Y. Zhang, and A. Taani. Constraints on Estimation of Radius of Double Pulsar PSR J0737-3039A and Its Neutron Star Nuclear Matter Composition. *Chinese Physics Letters*, 34(12):129701, 2017a.
- Y.-Y. Yang, C.-M. Zhang, D. Li, D.-H. Wang, Y.-Y. Pan, R.-F. Lingfu, and Z.-W. Zhou. Similarity of PSR J1906+0746 TO PSR J0737-3039: A Candidate of a New Double Pulsar System? *ApJ*, 835(2):185, 2017b.
- S. Zha, E. P. O’Connor, S. M. Couch, S.-C. Leung, and K. Nomoto. Hydrodynamic simulations of electron-capture supernovae: progenitor and dimension dependence. *MNRAS*, 513(1):1317–1328, 2022.
- C. M. Zhang and Y. Kojima. The bottom magnetic field and magnetosphere evolution of neutron star in low-mass X-ray binary. *MNRAS*, 366(1):137–143, 2006.
- C. M. Zhang, J. Wang, Y. H. Zhao, H. X. Yin, L. M. Song, D. P. Menezes, D. T. Wickramasinghe, L. Ferrario, and P. Chardonnet. Study of measured pulsar masses and their possible conclusions. *A&A*, 527:A83, 2011.
- X.-J. Zhu and G. Ashton. Characterizing Astrophysical Binary Neutron Stars with Gravitational Waves. *ApJ*, 902(1):L12, 2020.